Map-based Simulation Model for Energetic Assessment of Electric Propulsion Systems

(Article begins on next page)

Map-based Simulation Model for Energetic Assessment of Electric Propulsion Systems

Lorenzo Perilli
Student Member, IEEE
Dipartimento Energia
Politecnico di Torino
Turin, Italy
lorenzo.perilli@polito.it

Federica Graffeo
Member, IEEE
Dipartimento Energia
Politecnico di Torino
Turin, Italy
federica.graffeo@polito.it

Silvio Vaschetto
Senior Member, IEEE
Dipartimento Energia
Politecnico di Torino
Turin, Italy
silvio.vaschetto@polito.it

Alberto Tenconi
Senior Member, IEEE
Dipartimento Energia
Politecnico di Torino
Turin, Italy
alberto.tenconi@polito.it

***Abstract*—The electric propulsion systems modeling is a necessary tool for the evaluation of performance and onboard energy source requirements in electrically propelled aircraft. This paper presents a map-based simulation approach for energetic assessment of electric propulsion units, suitable for general aviation applications. The energetic analysis of the propulsion system relies on multidimensional maps to include the nonlinearities of the components, and the system dynamics is simulated by means of numerical integration. Additionally, the proposed approach considers the effects of electric machine temperature variations through a first-order thermal model. The developed model has been numerically validated in a simulation environment using the specifications of a commercial general aviation fuel aircraft.**

Keywords—transportation electrification, general aviation, electric aircraft, electric propulsion, energetic assessment, numerical simulation.

I. INTRODUCTION

The environmental concerns of the last decades have made carbon dioxide and nitrogen oxides emissions gain increasing attention from the public opinion. The largest government bodies and transnational companies are leading the transition toward sustainable and energy-efficient transportation as an effective solution to cope with climate change and global warming. Research activities on transportation environmental performance have been a key point of the recent European innovation programs. For instance, with its Climate Law, the EU has set legally binding targets to meet the greenhouse gas neutrality requirements by the end of 2050 [1]. In 2022, the aerospace industry was responsible for 13.3% of the EU transport gas emissions [2]. According to the International Air Transport Association, an 80% share of the carbon emissions occurs on flight paths longer than 1500 km [3]. Therefore, the electric aircraft development is a crucial feature to enable the decarbonization of the air transport sector.

In this scenario, the basis for a long-term transition from onboard non-propulsive mechanical, hydraulic and pneumatic systems to electrical ones has been set by the concept of More Electric Aircraft (MEA) [4]. With the ultimate goal being the achievement of the electrically propelled aircraft, interest in high-performance electric propulsion components has also arisen [5]. Indeed, an electric drive as propulsion system could provide reduced air pollutant emissions and acoustic noise, and enable highly efficient energy conversion, with respect to the traditional fuel-based units. Several proposals for electric machines and power electronics converter configurations for power dense aerospace drives can be found in the literature [6]-[7]. The major challenges are represented by weight and technology readiness level of the aerospace electric drives, presently limiting advancement of passenger class electrically propelled aircraft for commercial missions [8]. In this regard, the development of enabling technologies for general aviation purposes could allow significant progress in civil aviation.

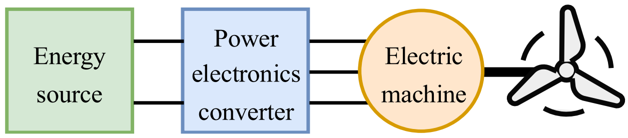

Fig. 1. Reference propulsion architecture for the model development.

To assess the feasibility of electrically propelled general aviation aircraft, numerical simulations play a fundamental role in predicting flight ranges and energy consumption of electric propulsion systems. In addition to that, numerical simulations constitute a preliminary step before proceeding with extensive optimization studies of the electric propulsion systems. A typical configuration for a fully electric general aviation propulsion unit is presented in Fig. 1. The onboard energy source provides power to the electric drive, i.e., the combination of the power electronics converter and of the electric machine, to spin the propeller, being the vast majority of general aviation aircraft propeller powered [9].

The simulation results accuracy for energetic assessment of these electric propulsion configurations can benefit from the implementation of multidimensional performance maps into the numerical model. In that case, the nonlinear behavior of the electric drive components would be formulated as a function of the power required by the propeller. To further improve the modeling accuracy, it is possible to consider the electric machine performance dependance on the active parts temperature, in addition to the load speed and to the required output torque. The numerical computation of the machine thermal transient provides the multidimensional performance maps with the temperature information. Regarding the power electronics converter, its operation is strictly related to the control strategy chosen for the electric drive. The converter power losses can be determined as a function of machine terminals voltages, currents and power factors, for a fixed temperature and working point. Moreover, improved accuracy of the electric drive simulation can be achieved considering the impact that variations in the remaining energy stored in the onboard source have on the adopted control strategy, through variations in the available voltage level.

In this paper, a map-based approach for simulating the energy consumption of fully electric propulsion systems for general aviation aircraft is proposed. The electric machine operational constraints for the output torque generation are taken into account by means of multidimensional maps, to model their dependencies on rotational speed, temperature and available source voltage. A machine first-order thermal model is also included to simulate the thermal transient during the flight mission. Additionally, the energetic performance of the electric drive components is assessed using multidimensional maps. The map-based approach provides the electric drive model with increased flexibility in simulating a wide range of electric machines and power electronics converters.

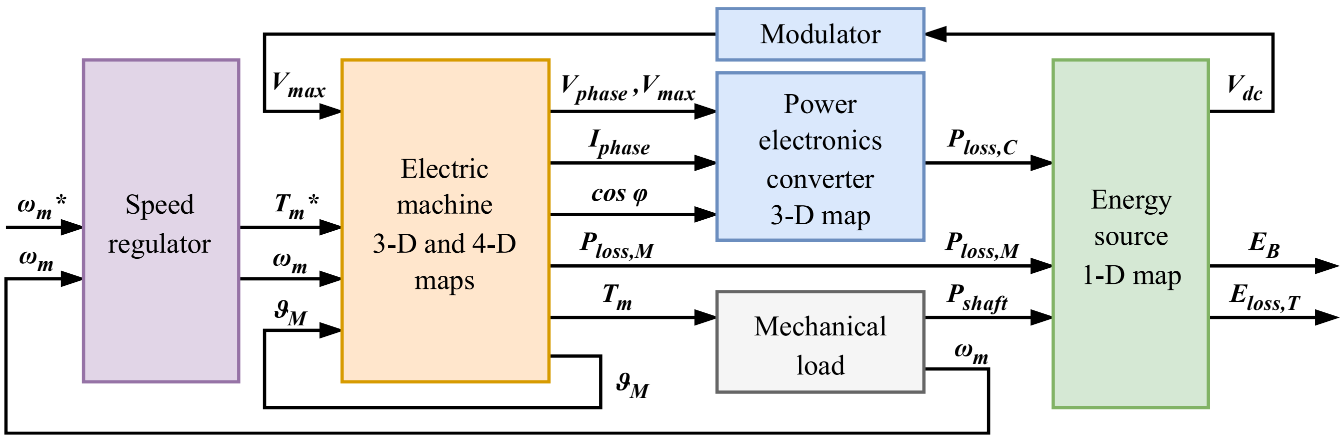

Fig. 2. Scheme of the proposed simulation model with the input and output signals linking the different components blocks.

II. Simulation Approaches

In the literature, two general approaches can be found for determining energy consumption and flight ranges [10]-[11]. The first one consists of the backward model, in which the reference speed profile of the propeller is assumed to be perfectly followed by propulsion unit. At every time instant, the power needed for spinning the propeller is computed by means of algebraic equations and the propulsion system is assumed to be certainly able to provide it. Since the power information is propagated from the mechanical load to the propulsion unit, the approach is usually called *'backward'*. This method is mostly adopted for comparing energy source control strategies and propulsion system configurations [12]. However, since both the speed and power are simultaneously imposed on the powertrain components, the simulation results may be inaccurate when the components ratings are exceeded [13].

The second approach for propulsion systems simulation relies on the forward model. In this case, the propeller speed is controlled in closed-loop by means of a regulator, which generates the torque reference signal for the propulsion unit. Such approach is commonly referred to as *'forward'*, since the power signal is passed from the propulsion unit to the load. The propeller speed is a state variable of the model and is updated at every simulation step. Being the forward model characterized by a set of differential equations, the numerical solution requires smaller time steps compared to the backward approach, resulting in a longer execution time. Nevertheless, the forward method allows to consider the performance limits and the dynamic behavior of the components in the propulsion system. For these reasons, the forward method is suitable for Hardware-in-the-Loop validation, in contrast to the backward one [14]-[15].

III. Proposed Simulation Model

The proposed model for the evaluation of the electric propulsion systems performance and energy consumption is based on the forward approach and is presented in Fig. 2. The speed regulator provides the reference torque signal to the electric machine block, in order to follow the propeller reference speed profile. The interpolation of the electric machine 3-D and 4-D maps generates the inputs for the computation of the power electronics converter losses. The information of the mechanical power delivered to the load, together with the electric drive losses, is passed to the energy source block for the energy requirements assessment through numerical integration.

A. Speed Regulator

Being the proposed model based on the forward approach, a speed regulator is necessary to control the propeller speed. As shown in Fig. 2, the speed regulator block inputs are the propeller reference ω_m^* and actual ω_m speeds, respectively. An effective method to control the propeller speed consists of a PI regulator. The comparison of the reference signal with the actual propeller speed is used to generate an error. By means of the proportional K_P and integral K_I gains, a reference torque T_m^* output signal is produced by the regulator block for the electric machine, according to the following equation:

$$T_m^* = \left(K_P + \frac{K_I}{s}\right)(\omega_m^* - \omega_m) \tag{1}$$

in which s is the Laplace frequency domain parameter.

B. Electric machine

The electric machine model is thoroughly presented in Fig. 3. The first-order low-pass filter (2) with time constant τ_M implements the drive delay in tracking the reference torque, and its output is limited by a saturation block, to numerically consider the machine performance limits.

$$T_m' = \frac{1}{1+s\tau_M} T_m^* \tag{2}$$

The torque upper and lower boundaries for saturating the filter output T_m' are retrieved from the following 3-D maps:

$$T_{m,max} = T_{m,max}(\omega_m, \vartheta_M, V_{max}) \tag{3}$$

$$T_{m,min} = T_{m,min}(\omega_m, \vartheta_M, V_{max}) \tag{4}$$

where ϑ_M is the electric machine temperature and V_{max} is the maximum output voltage available at the terminals of the power converter. The torque information is passed to the other electric machine 4-D maps and to the mechanical load block.

The terminals voltages, currents and power factors needed for all the electric machine feasible operating points and the losses are retrieved by means of 4-D maps, as shown in Fig. 3. Such maps can be determined either by finite element analysis (FEA) or experimental tests. According to the chosen control strategy (maximum torque per ampere, maximum efficiency per torque, etc.), different 4-D maps can be determined for the machine simulation. Indeed, the same working point in the torque-speed plane can be obtained for different combinations of the electrical quantities. The voltage and current amplitudes V_{phase} and I_{phase} and the power factor $\cos\varphi$ outputs are used for the interpolation of the power electronics converter maps.

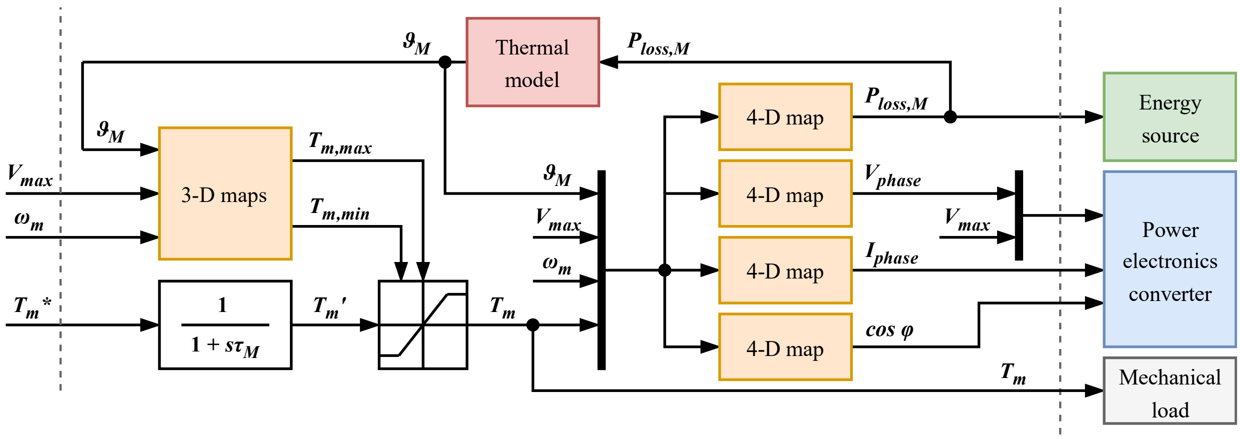

Fig. 3. Detailed scheme of the proposed electric machine energetic model.

With regard to the energetic performance of the electric machine, the 4-D losses map provides the component losses $P_{loss,M}$ to the thermal model and the energy source block. The usage of losses rather than efficiency maps for determining the energy consumption is a convenient practice, since efficiency becomes ill defined when either the machine speed or the torque are null. Moreover, the losses maps allow to take into account the losses present at zero speed or torque and to reduce the simulation burden, as the energy computation is performed through sums, instead of products and divisions.

The machine output torque, speed and temperature, as well as the V_{max} value, are used as inputs to the 4-D losses, voltage, current and power factor maps, as shown in Fig. 3, which are formulated as follows:

$$P_{loss,M} = P_{loss,M}(T_m, \omega_m, \vartheta_M, V_{max}) \quad (5)$$

$$V_{phase} = V_{phase}(T_m, \omega_m, \vartheta_M, V_{max}) \quad (6)$$

$$I_{phase} = I_{phase}(T_m, \omega_m, \vartheta_M, V_{max}) \quad (7)$$

$$\cos\varphi = \cos\varphi\,(T_m, \omega_m, \vartheta_M, V_{max}) \quad (8)$$

The ϑ_M dependency in (5)-(8) allows to take into account the changes in the machine windings resistances, but also in the residual magnetization of any permanent magnet, due to temperature variations. The machine temperature is retrieved from a first-order thermal model, shown in Fig. 4, for which the machine is considered as a homogeneous cylinder with thermal capacitance $C_{th,M}$ and resistance $R_{th,M}$. Being ϑ_{amb} the ambient temperature, the electric machine temperature is updated in the numerical simulation by integration of (9).

$$\frac{d\vartheta_M}{dt} = \frac{1}{C_{th,M}}\left(P_{loss,M} - \frac{\vartheta_M - \vartheta_{amb}}{R_{th,M}}\right) \quad (9)$$

C. Power electronics converter and modulator

The energetic performance of the power electronics converter depends on the voltage, current and power factor required at the machine terminals. Moreover, the converter losses are also influenced by the V_{dc} level provided by the energy source and by the devices switching frequency f_{sw}.

For a fixed value of the switching frequency, the power converter model for energy consumption simulations can be developed as a single 3-D map, in the form:

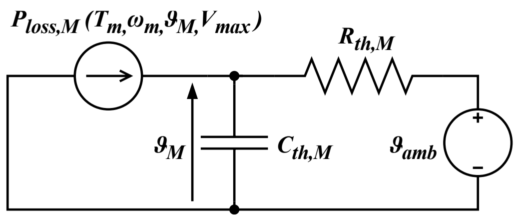

Fig. 4. First-order thermal model for the electric machine.

$$P_{loss,C} = P_{loss,C}(m, I_{phase}, \cos\varphi) \quad (10)$$

where $P_{loss,C}$ are the converter losses, depending on the modulation index m, defined as in (11), being V_{dc} the voltage at the energy source terminals.

$$m = 2\frac{V_{phase}}{V_{dc}} \quad (11)$$

The modulation index value m_{max} up to which the power converter losses map has to be characterized is determined from the adopted modulation technique. For a three-phase, two-level, voltage source inverter supplying a synchronous machine, typical values of m_{max} are 1 for sinusoidal pulse width modulation (PWM) and $2/\sqrt{3}$ for space vector and carrier-based PWM [16]-[17].

The modulator block in Fig. 2 is needed to compute the maximum voltage V_{max} available at the electric machine terminals, for the machine 3-D and 4-D maps interpolation. According to the modulation technique chosen for the power electronics converter, m_{max} is used to retrieve V_{max} from the voltage at the energy source terminals by means of (12).

$$V_{max} = \frac{V_{dc}}{2} m_{max} \quad (12)$$

D. Mechanical load

The mechanical load block performs the integration of (13) at every simulation step, to compute the actual rotational speed of the electric machine and mechanical load.

$$\frac{d\omega_m}{dt} = \frac{T_m - T_{load}}{J_{eq}} \quad (13)$$

As shown in Fig. 2, the ω_m signal is passed to the speed regulator block for the reference torque calculation, and to the electric machine 3-D and 4-D maps. In (13), the equivalent moment of inertia J_{eq} of the machine rotor-load coupling is

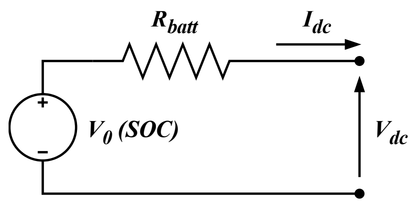

Fig. 5. Battery circuital model for the propulsion system simulation.

referred to the rotational axis of the machine shaft and T_{load} is the load torque, generally a function of its rotational speed:

$$T_{load} = T_{load}(\omega_m) \tag{14}$$

Depending on the load model, different formulations can be used for (14). For the general aviation propulsion system configuration presented in Fig. 1, the load is represented by a propeller, with radius r_{prop}. Given a constant value for the air density ρ_{air}, the propeller load torque can be formulated as:

$$T_{load} = \rho_{air} C_Q r_{prop}^5 \omega_m^2 \tag{15}$$

in which C_Q denotes the propeller torque coefficient [18]. A more accurate formulation of (15) could be introduced in the model by considering the dependencies of ρ_{air} on the aircraft altitude and of C_Q on advance ratio and blades pitch [19]. In this paper, a constant parameters formulation of (15) is considered to simulate the proposed model.

E. Energy source

The energy source model takes into account the nonlinear operation of the component, with reference to the available output voltage, as a function of the remaining stored energy, regardless the energy source type. As it can be noted in Fig. 2, the 1-D map of the energy source block must provide the voltage V_{dc} at its terminals to the modulator block for the V_{max} computation, conditioning the electric machine and the power electronics converter performance. The source dynamics in delivering power to the electric drive has not been considered in the proposed model. The energy source block presents also as inputs the power for spinning the propeller and the drive components power losses, in order to update the energy level and to perform the power integration.

A possible model for an energy source consisting of a single battery is proposed in Fig. 5. The nonlinear behavior is considered by means of the 1-D map in (16), which relates the battery state of charge SOC to its open-circuit voltage V_0.

$$V_0 = V_0(SOC) \tag{16}$$

Regarding the solution algorithm for the battery model, by defining the mechanical power at the machine shaft as in (17), the energy source current I_{dc} is computed by means of (18).

$$P_{shaft} = T_m \omega_m \tag{17}$$

$$I_{dc} = \frac{P_{shaft} + P_{loss,M} + P_{loss,C}}{V_{dc}} \tag{18}$$

Therefore, the voltage available at the source terminals is retrieved from:

$$V_{dc} = V_0 - R_{batt} I_{dc} \tag{19}$$

where R_{batt} denotes the battery internal resistance [20].

Finally, the battery losses $P_{loss,S}$ can be computed from (20).

$$P_{loss,S} = R_{batt} I_{dc}^2 \tag{20}$$

In order to take into account the performance variation of the battery as a function of the SOC, the following equation is numerically integrated to update the SOC value:

$$\frac{dSOC}{dt} = -\frac{i_{dc}}{C_{batt}} \tag{21}$$

in which C_{batt} is the rated battery capacity.

The energy source block implements also the numerical integration of the mechanical power (17) and of the total system losses, computed as in (22).

$$P_{loss,T} = P_{loss,M} + P_{loss,C} + P_{loss,S} \tag{22}$$

The total energy $E_{loss,T}$ lost by the propulsion components during the mission profile and the corresponding energy E_B requested to the source are determined using (23)-(24).

$$E_{loss,T} = \int_0^t P_{loss,T}\, dt \tag{23}$$

$$E_B = E_{loss,T} + \int_0^t P_{shaft}\, dt \tag{24}$$

IV. Maps Identification and Example of Results for a Case Study

The proposed model has been used for the numerical computation of the energetic consumption of an electrically propelled case study aircraft for general aviation applications. A propulsion system featuring the fully electric configuration presented in Fig. 1 has been considered for the specifications of a commercial general aviation fuel aircraft.

For the model validation, a 250 kW air-cooled surface-mounted permanent magnet synchronous machine has been designed by means of finite elements analysis. The machine features a distributed three-phase stator winding, an outer rotor with NdFeB permanent magnets and 8 poles. The post-elaboration of the machine FEA results has provided the 3-D and 4-D maps of the model depicted in Fig. 3.

The machine 4-D maps have been derived according to the maximum efficiency per torque control strategy, for a grid of 201 torque and 101 speed values, temperatures from 5°C to 155°C with steps of 15°C and for a set of 10 levels of V_{max} corresponding to values from 100% to 10% of the battery SOC. The results obtained for a machine temperature of 20°C and maximum source voltage are shown in Fig. 6. The losses map includes the hysteresis and eddy currents losses of the stator and rotor iron cores, the permanent magnets losses and the Joule losses of the stator windings, while the AC losses related to the skin and proximity effects, the PWM losses and the machine mechanical losses have been disregarded [21].

The adopted control strategy has also determined the machine maximum (3) and minimum (4) torque maps, with T_{max} shown in Fig. 7. As it is evident from the maximum torque limit, when the source discharges and the available voltage at its terminal lowers, working points are ruled out from the feasible operation of the machine, due to voltage limitations [22]-[23]. Moreover, being the chosen permanent magnets characterized by a negative residual magnetization temperature coefficient of −0.11%/°C, the machine torque capability worsens as their temperature rises. In this case,

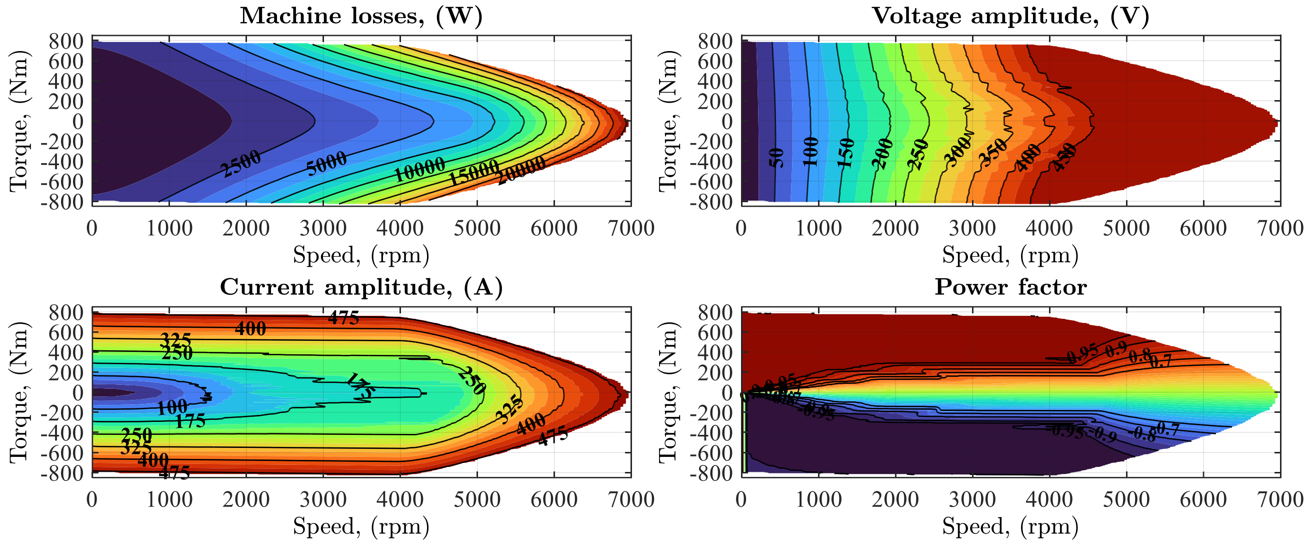

Fig. 6. Electric machine 4-D maps at 20°C and maximum source voltage for the simulation of the proposed forward model.

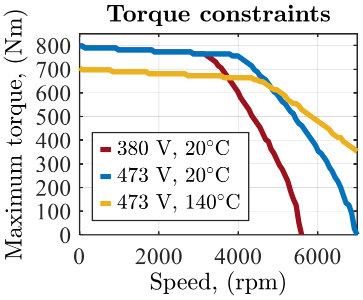

Fig. 7. Torque boundaries for different voltages and temperatures.

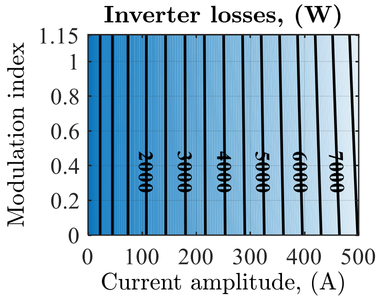

Fig. 8. Inverter losses map for a load power factor value of 0.9.

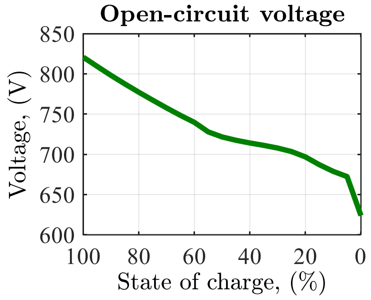

Fig. 9. Battery 1-D map for the open-circuit voltage determination.

working points are ruled out due to current limitations, as shown in Fig. 7. Furthermore, the $R_{th,M}$ of the first-order machine thermal model showcases the approach capabilities, ensuring that the machine active parts temperature remains under 140°C when the propeller is spun at nominal speed.

Concerning the power electronics converter, the 3-D map of the model in Fig. 2 has been computed through numerical simulations. For the general aviation case study, the tabulated data of the nonlinear voltage drops and losses in commercial power electronics devices have been considered for a two-level, three-phase IGBT inverter. According to [24]-[25], the conduction and switching losses of the power devices can be numerically determined for sets of modulation index, current amplitude and load power factor values. The resulting losses map of the inverter for devices with a temperature of 150°C is presented in Fig. 8, at load power factor equal to 0.9. The chosen maximum current amplitude is in accordance with the I_{phase} of the machine, while the maximum value of m in the map corresponds to the space vector and carrier-based PWM techniques. The different modulation indices are simulated by varying only V_{phase}, keeping V_{max} at its maximum value, corresponding to the 100% battery SOC. An f_{sw} of 20 kHz has been chosen for the inverter operation and characterization.

Regarding the onboard energy source, a battery has been considered starting from the datasheet of a commercial Li-ion cell. The 1-D map (16) for the determination of the open-circuit voltage is presented in Fig. 9. The battery nominal V_{dc} allows the inverter to supply the machine with its nominal current, when the SOC is 50% or more. Moreover, the number of parallel connected cells ensures that the remaining SOC at the end of the reference speed profile is not lower than 10%.

The reference speed profile for the propeller used in the model validation consists of four parts. As it can be seen in Fig. 10, the profile includes (i) taxiing, (ii) takeoff and climbing, (iii) cruise, (iv) descent and landing. The numerical simulation has been performed using a 4-th order Runge-Kutta method with a fixed step of 0.01 s. The representative evolution of the most significant variables, such as the energy requested to the source during the flight and the total energy lost, is presented in Fig. 10, along with the battery SOC, the reference torque from the regulator, the machine shaft torque and its temperature. However, the drive dynamics in tracking the torque reference is not evident in Fig. 10 due to the time scale, as it affects the speed transients. It is also worth noting that, as it has been assumed for the propeller load torque, the effects of altitude variations on the ambient temperature of the machine thermal model have not been implemented.

V. Conclusion

A map-based simulation model for energetic assessment of fully electric general aviation propulsion systems has been developed and validated through numerical simulations. The proposed tool can be beneficial to research activities on the electrification of the air transport sector.

In the presented forward approach, the performance of electric machine and power electronics converter is simulated by means of 3-D and 4-D maps. The propulsion system limits are considered through torque boundaries maps, preventing data extrapolation and improving simulation results accuracy. In addition, the electric drive dynamics is taken into account by introducing a first-order low-pass filter, representing the drive delay in tracking the reference torque signal. A machine

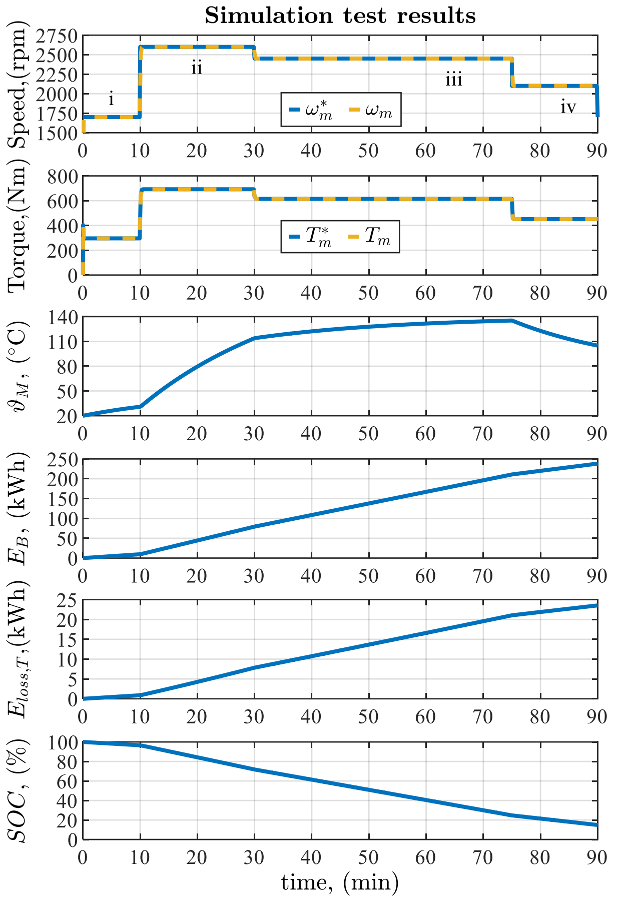

Fig. 10. Simulation results for a 90 min flight including taxiing, takeoff, cruise and landing.

thermal model of the first order is also included for updating the active parts temperature at every simulation step.

A simulation test has been carried out using a surface PM synchronous machine and a two-level, three-phase inverter. The losses maps have been computed numerically for both the components, along with the 3-D torque boundaries of the electric machine and 4-D voltage, current and power factor maps. The nonlinear relationship between the battery state of charge and the open-circuit voltage has been also considered in the numerical environment. The map-based modeling approach allows for flexibility in simulating a wide range of machines and power electronics converters. More accurate and complex models for the energy source and propeller can also be implemented in the proposed approach to achieve improved accuracy in the numerical results.

Acknowledgments

This study was carried out within the MOST – Sustainable Mobility National Research Center and received funding from the European Union Next-GenerationEU (PIANO NAZIONALE DI RIPRESA E RESILIENZA (PNRR) – MISSIONE 4 COMPONENTE 2, INVESTIMENTO 1.4 – D.D. 1033 17/06/2022, CN00000023). This manuscript reflects only the authors' views and opinions, neither the European Union nor the European Commission can be considered responsible for them.

This publication is part of the project PNRR-NGEU which has received funding from the MUR-DM 117/2023.

References

[1] https://climate.ec.europa.eu/eu-action/european-climate-law_en
[2] https://www.europarl.europa.eu/topics/en/topic/climate-change
[3] https://www.iata.org/en/youandiata/travelers/environment
[4] W. Cao, B. C. Mecrow, G. J. Atkinson, J. W. Bennett and D. J. Atkinson, "Overview of Electric Motor Technologies Used for More Electric Aircraft (MEA)," *IEEE Trans. Ind. Electron.*, vol. 59, no. 9, pp. 3523-3531, Sept. 2012.
[5] X. Zhang, C. L. Bowman, T. C. O'Connell and K. S. Haran, "Large electric machines for aircraft electric propulsion," in *IET Electric Power Applications*, 12: 767-779, 2018.
[6] A. Del Pizzo, L. P. Di Noia and A. Pizza, "Analysis of a five phase electrical drive for the propulsion of all electric aircraft," 2016 AEIT International Annual Conference (AEIT), Capri, Italy, 2016, pp. 1-6.
[7] D. Golovanov, D. Gerada, Z. Xu, C. Gerada, A. Page and T. Sawata, "Designing an Advanced Electrical Motor for Propulsion of Electric Aircraft," 2019 AIAA/IEEE Electric Aircraft Technologies Symposium (EATS), Indianapolis, IN, USA, 2019, pp. 1-12.
[8] A. Barzkar and M. Ghassemi, "Components of Electrical Power Systems in More and All-Electric Aircraft: A Review," *IEEE Trans. Transp. Electrif.*, vol. 8, no. 4, pp. 4037-4053, Dec. 2022.
[9] R. Jeracki and G. Mitchell, "Low and High Speed Propellers for General Aviation — Performance Potential and Recent Wind Tunnel Test Results," SAE Technical Paper 811090, 1981.
[10] A. Gurusamy, B. Ashok and B. Mason, "Prediction of Electric Vehicle Driving Range and Performance Characteristics: A Review on Analytical Modeling Strategies With Its Influential Factors and Improvisation Techniques," in *IEEE Access*, vol. 11, 2023.
[11] K. B. Wipke, M. R. Cuddy and S. D. Burch, "ADVISOR 2.1: a user-friendly advanced powertrain simulation using a combined backward/forward approach," *IEEE Trans. Veh. Technol.*, vol. 48, no. 6, pp. 1751-1761, Nov. 1999.
[12] P. Pettersson, B. Jacobson, F. Bruzelius, P. Johannesson, and L. Fast, "Intrinsic differences between backward and forward vehicle simulation models," *IFAC-PapersOnLine*, vol. 53, no. 2, 2020.
[13] G. Mohan, F. Assadian and S. Longo, "Comparative analysis of forward-facing models vs backwardfacing models in powertrain component sizing," IET Hybrid and Electric Vehicles Conf., 2013.
[14] Z. Filipi, H. Fathy, J. Hagena, A. Knafl, R. Ahlawat, J. Liu, D. Jung, D. Assanis, H. Peng and J. Stein, "Engine-in-the-Loop Testing for Evaluating Hybrid Propulsion Concepts and Transient Emissions – HMMWV Case Study," SAE Technical Paper 2006-01-0443, 2006.
[15] P. Poletto, A. Angiolini, G. Boccardo, E. Graziano, S. Vaschetto and R. Demelas, "Real Time Modelling of Automotive Electric Drives for Hardware-in-the-Loop Applications," SAE Technical Paper 2023-24-0028, 2023.
[16] D. G. Holmes, "The significance of zero space vector placement for carrier-based PWM schemes," *IEEE Trans. Ind. Appl.*, vol. 32, no. 5, pp. 1122-1129, Sept.-Oct. 1996.
[17] K. Zhou and D. Wang, "Relationship between space-vector modulation and three-phase carrier-based PWM: a comprehensive analysis," *IEEE Trans. Ind. Electron.*, vol. 49, no. 1, pp. 186-196, Feb. 2002.
[18] D. Lawhorn, V. Rallabandi and D. M. Ionel, "Electric Aircraft System Co-Simulation Including Body, Propeller, Propulsion, and Energy Storage Models," 2019 IEEE Transportation Electrification Conference and Expo (ITEC), Detroit, MI, USA, 2019, pp. 1-5.
[19] M. M. Rivera and L. B. Gutiérrez, "Dynamic model of an aircraft propulsion system with electric motor and propeller," 2021 IEEE 5th Colombian Conference on Automatic Control (CCAC), 2021.
[20] F. L. Mapelli, D. Tarsitano and M. Mauri, "Plug-In Hybrid Electric Vehicle: Modeling, Prototype Realization, and Inverter Losses Reduction Analysis," *IEEE Trans. Ind. Electron.*, vol. 57, no. 2, pp. 598-607, Feb. 2010.
[21] A. Mahmoudi, W. L. Soong, G. Pellegrino and E. Armando, "Efficiency maps of electrical machines," IEEE-ECCE, 2015.
[22] O. Stiscia, S. Rubino, S. Vaschetto, A. Cavagnino and A. Tenconi, "Accurate Induction Machines Efficiency Mapping Computed by Standard Test Parameters," *IEEE Trans. Ind. Appl.*, vol. 58, no. 3, pp. 3522-3532, May-June 2022.
[23] O. Stiscia, S. Rubino, S. Vaschetto, A. Cavagnino and A. Tenconi, "Off-Line Efficiency Mapping of Induction Motors Operated in Wide Torque-Speed Ranges," IEEE-ECCE, 2020.
[24] C. Axtmann, J. Kolb and M. Braum, "Efficiency map computation of arbitrary converter topologies in EV powertrains," 2016 IEEE 2nd Annual Southern Power Electronics Conference (SPEC), 2016.
[25] J. W. Kolar, H. Ertl and F. C. Zach, "Calculation of the Passive and Active Component Stress of Three-Phase PWM Converter Systems with High Pulse Rate", Proceedings of the 3rd European Conference on Power Electronics and Applications, vol. 3, pp. 1303-1311, Oct. 1989.